

# Effect of wavelength dependence of nonlinearity, gain, and dispersion in photonic crystal fiber amplifiers

A. Huttunen<sup>1</sup> and P. Törmä<sup>2</sup>

<sup>1</sup>*Department of Electrical and Communications Engineering, Laboratory of Computational Engineering, Helsinki University of Technology, FIN-02015 HUT, Finland\**

<sup>2</sup>*Department of Physics, Nanoscience Center, FIN-40014 University of Jyväskylä, Finland*

Photonic crystal fibers are used in fiber amplifiers and lasers because of the flexibility in the design of mode area and dispersion. However, these quantities depend strongly on the wavelength. The wavelength dependence of gain, nonlinearity and dispersion are investigated here by including the wavelength dependence explicitly in the nonlinear Schrödinger equation for photonic crystal fibers with varying periods and hole sizes. The effect of the wavelength dependence of each parameter is studied separately as well as combined. The wavelength dependence of the parameters is shown to create asymmetry to the spectrum and chirp, but to have a moderating effect on pulse broadening. The effect of including the wavelength dependence of nonlinearity in the simulations is demonstrated to be the most significant compared that of dispersion or gain.

PACS numbers:

## INTRODUCTION

Photonic crystal fibers are a new class of optical fibers that have a periodic cladding [1, 2]. Light can be confined to the core either by the band gap effect or by total internal reflection by average refractive index difference. Photonic crystal fibers have many intriguing characteristics, for example, they can be endlessly single mode, have extremely small or large mode areas and still remain single mode. Also the dispersion properties of photonic crystal fibers are very different from standard optical fiber. The research of photonic crystal fiber lasers [3, 4, 5, 6, 7, 8, 9, 10, 11, 12, 13, 14, 15, 16] and amplifiers [17, 18, 19, 20, 21, 22, 23, 24] has been intense in the past few years. The aim has been two-fold. First, the possibility of obtaining a small mode area has been exploited by designing high-gain amplifiers/lasers where the overlap between the mode distribution and doped area is maximized. On the other hand, the possibility of obtaining a large mode area has been utilized for realizing high-power amplifiers/lasers with low nonlinearity.

Small-mode area photonic crystal fibers generally have large dispersion and nonlinearity that also depend strongly on the wavelength [25]. In this paper, we study the propagation of 200 fs pulses in high-gain small-mode area photonic crystal fiber amplifiers. When short pulses are considered, the spectrum is wide and thus the wavelength dependence of the different parameters has a profound effect on the pulse propagation.

We compare the temporal and spectral widths, time-bandwidth products, and chirps of the pulses and amplification properties for different fiber geometries. We find out that the wavelength dependence of the parameters has a substantial effect on the pulse properties after it has propagated a short distance in the fiber amplifier. The dispersion caused by the wavelength dependence of the nonlinearity counteracts the dispersion of

the fiber and thus the pulses do not broaden as much as it is expected by considering constant parameter values for dispersion and nonlinearity. On the other hand, the spectral broadening and chirping become asymmetric when the wavelength dependence of the parameters is taken into account. Also, the wavelength dependence of the dispersion parameters and gain is seen to influence the pulse quality less, compared to the important effect of wavelength dependence of nonlinearity, indicating that in some cases they could be approximated by constant values when simulating pulse propagation in photonic crystal fibers.

## NUMERICAL METHODS

The pulse propagation is studied with the optical nonlinear Schrödinger equation

$$\frac{\partial A}{\partial z} = - \sum_{m=1}^4 \frac{i^{m+1}}{m!} \beta_m \frac{\partial^m A}{\partial T^m} + \frac{gA}{2} + i\gamma \left( 1 + \frac{i}{\omega_0} \frac{\partial}{\partial T} \right) A \int_{-\infty}^{\infty} R(T') |A(z, T - T')|^2 dT', \quad (1)$$

which is simulated by the split-step Fourier method [26]. The parameters for gain, nonlinearity and dispersion are taken to be either constants  $g$ ,  $\gamma$  and  $\beta_m$  or wavelength dependent  $g(\lambda)$ ,  $\gamma(\lambda)$  and  $\beta_m(\lambda)$ , respectively. The slowly varying envelope of the pulse is taken to be Gaussian

$$A(z=0, T) = \sqrt{P_0} e^{-T^2/(2T_0^2)}, \quad (2)$$

where  $P_0$  is the peak power and  $T_0$  is the pulse length.

The values of the dispersion and nonlinear parameters are calculated as explained in Ref. [27]. The dispersion

parameters  $\beta_m$  are defined as

$$\beta_m = \left[ \frac{d^m \beta}{d\omega^m} \right]. \quad (3)$$

The mode-propagation constants  $\beta$  as a function of the frequency  $\omega$  were calculated with the full-vectorial plane wave method (the MIT Photonic bands software) [28]. The nonlinear parameter

$$\gamma(\lambda) = \frac{2\pi}{\lambda} \frac{n_2}{A_{\text{eff}}(\lambda)}, \quad (4)$$

is inversely proportional to the effective area, which is calculated from the intensity distribution of the eigenmode

$$A_{\text{eff}}(\lambda) = \frac{[\int I(r)dr]^2}{\int I^2(r)dr} \quad (5)$$

and  $n_2$  is the nonlinear-index coefficient  $n_2 = 3 \cdot 10^{-20} \text{m}^2/\text{W}$ .

We consider an Erbium-doped fiber amplifier. The gain as a function of wavelength is as in Fig. 1 of Ref. [22] and it is approximated to be the same for all geometries since it has the least effect on the pulse propagation characteristics such as pulse broadening. Also, according to Ref. [18] the gain dependence on the wavelength is strongly influenced by the emission and absorption cross section rather than by the photonic crystal fiber geometry.

### THE STUDIED FIBER GEOMETRIES AND PULSE PROPERTIES

We investigate photonic crystal fibers with a triangular lattice of air holes in the cladding. The core is formed by a missing hole. We consider geometries with the hole diameter to period ratios  $d/P = 0.2, 0.3, 0.4, 0.5, 0.6$  and periods  $P = 2, 3, 4, 5, 6 \mu\text{m}$ . The geometries are those of interest in the research on high-gain efficiency photonic crystal fiber amplifiers [15, 19, 21, 22]. The dispersion and nonlinear parameters [see Eqs. (3) and (4)] are calculated as a function of the wavelength for all the geometries. They are shown in Fig. 1 for the fiber geometry  $d/P = 0.3$ .

The magnitude of the period affects the wavelength dependence of the  $\beta_m$ . Regardless of  $d/P$ , for  $P = 2 \mu\text{m}$ , the  $\beta_m$  are strongly dependent on the wavelength while for  $P = 6 \mu\text{m}$  the wavelength dependence is not as prominent. The functional form of the  $\beta_m$  as a function of the wavelength is very different for the different fiber geometries. For example, for  $P = 2 \mu\text{m}$ , the value of  $\beta_2$  in the center of the considered wavelength range is positive when  $d/P=0.2, 0.3$ , and  $0.4$ , but negative when  $d/P=0.5$  and  $0.6$ , which can affect the pulse propagation considerably. The nonlinear coefficient  $\gamma(\lambda)$ , however,

has a similar form as a function of wavelength for all fiber geometries. The steepness of  $\gamma(\lambda)$  increases when  $P$  decreases or  $d/P$  increases.

The studied pulse has the length 200 fs, wavelength  $1.55 \mu\text{m}$ , and peak power  $P_0 = 0.01 \text{ W}$ . The propagation distance is 10 cm. The time and frequency axis are divided into 4096 steps in the split-step Fourier-method.

To demonstrate the effect of the wavelength dependence of  $g(\lambda)$ ,  $\gamma(\lambda)$ , and  $\beta_m(\lambda)$  in Eq. (1), the simulations for all the different geometries are performed twice: with wavelength dependent gain, nonlinearity and dispersion parameters and, for comparison, with all these parameter values constant. The constant parameter values are determined at  $\lambda = 1.55 \mu\text{m}$ . The simulations for some of the geometries ( $d/P = 0.4$  and  $d/P = 0.5$ ) are repeated keeping the nonlinear parameter and gain wavelength dependent, but approximating the the dispersion parameters with constant values. Also, to investigate the effect of the wavelength dependence of gain, the simulations are repeated with all other parameters constant but including the wavelength dependence of gain.

### COMPARISON BETWEEN SIMULATIONS WITH CONSTANT AND WAVELENGTH DEPENDENT GAIN, NONLINEARITY, AND DISPERSION

We compare the simulations made with wavelength dependent and constant gain, nonlinear and dispersion parameters. After propagating 10 cm in the fiber amplifier, which is a short distance compared to actual amplifier lengths, there are clear differences for the two sets simulations. The pulse shape, spectrum, phase, and chirp are shown in Fig. 2 for one fiber geometry. The definitions of the phase of the pulse  $\phi$  and frequency chirp  $\delta\omega$  are

$$A(z, T) = |A(z, T)|e^{i\phi(z, T)} \quad (6)$$

$$\delta\omega = -\frac{\partial\phi}{\partial T}. \quad (7)$$

The chirp is a measure how much the instantaneous frequency changes across the pulse from the central frequency [26]. From Fig. 2 one can see that the self-steepening of the pulse is larger for the simulation with constant  $g$ ,  $\gamma$ , and  $\beta_m$  than for wavelength dependent  $g(\lambda)$ ,  $\gamma(\lambda)$ , and  $\beta_m(\lambda)$ . The spectrum of the pulse is more asymmetric when the wavelength dependence of the parameters is taken into account. Also, the chirp of the simulation with constant parameters is symmetric whereas the chirp of the one with the wavelength dependent parameters is larger (in absolute magnitude) on the leading edge of the pulse than on the trailing edge.

To characterize the pulses after the propagation in the amplifier, we calculate the temporal and spectral widths, time-bandwidth products, and chirps of the pulses as well

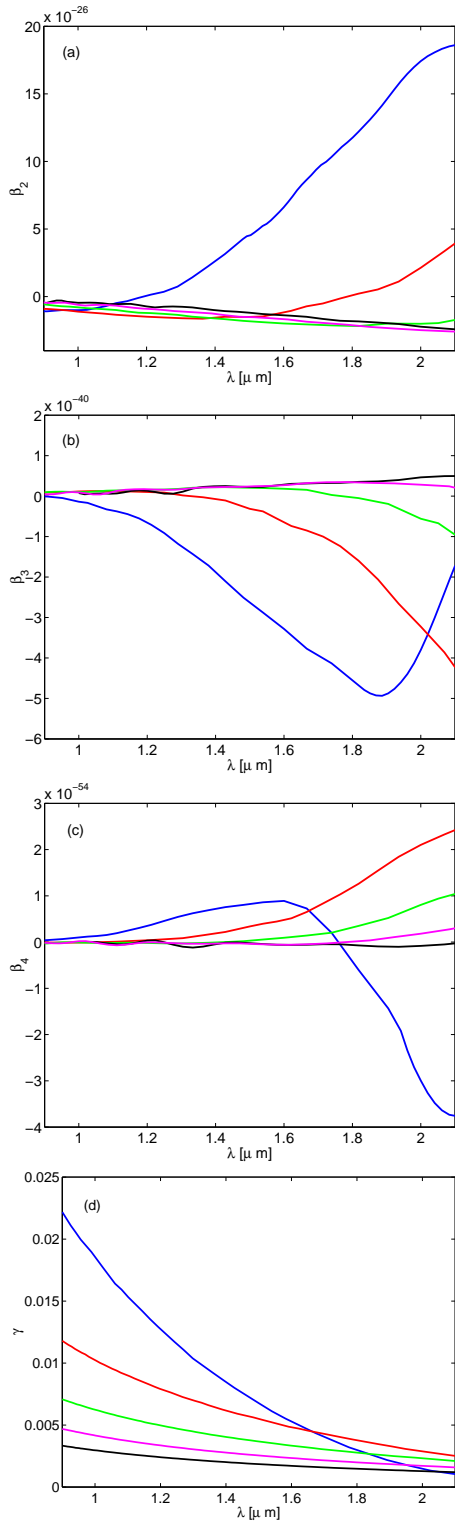


FIG. 1: Dispersion and nonlinear parameters as a function of wavelength for a photonic crystal fiber with  $d/P = 0.3$  and periods  $P = 2 \mu\text{m}$  (blue),  $P = 3 \mu\text{m}$  (red),  $P = 4 \mu\text{m}$  (green),  $P = 5 \mu\text{m}$  (magenta), and  $P = 6 \mu\text{m}$  (black).

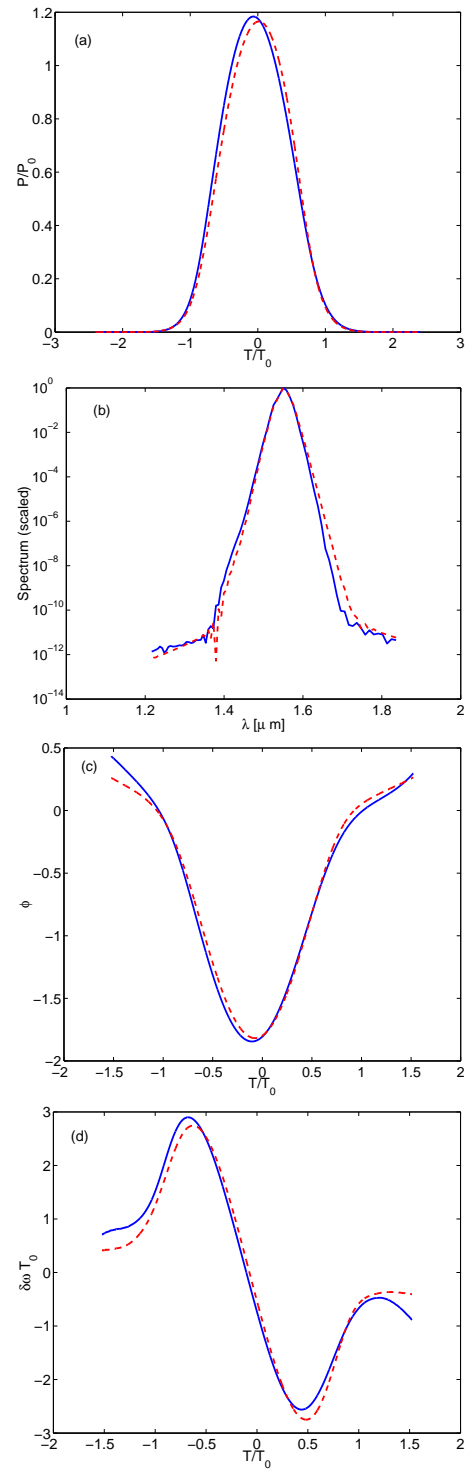


FIG. 2: (a) Pulse shape, (b) spectrum, (c) phase, and (d) chirp after it has propagated 10 cm in the fiber amplifier. The fiber geometry is  $d/P = 0.3$  and  $P = 3 \mu\text{m}$ . Blue curves represent the simulation with wavelength dependent parameters  $[g(\lambda), \gamma(\lambda), \beta_m(\lambda)]$  and red dashed curves with constant parameters ( $g, \gamma, \beta_m$ ). The propagation distance is short compared to the total lengths of the fiber amplifiers (which can be several meters).

as their amplification in the fiber. The temporal width is described by the full-width at half-maximum (FWHM) and denoted by  $\Delta T_{FWHM}$ . We also calculated the root-mean square widths of the pulses, but they are not shown here since there was no additional information compared to the FWHM widths. The spectral width is calculated as the full-width at half-maximum  $\Delta\omega_{FWHM}$ . The pulse widths, the time-bandwidth products

$$\text{TBP} = \frac{\Delta T_{FWHM} \Delta\omega_{FWHM}}{2\pi} \quad (8)$$

and the chirps are shown in Fig. 3 as a function of the period for the different fiber geometries. The chirp is indicated by the lowest value of the chirp [compare to Fig. 2(d)].

The results for constant and wavelength dependent  $g$ ,  $\gamma$ , and  $\beta_m$  are different. Pulses broaden less when the wavelength dependence of the parameters is taken into account, for all fiber geometries except  $d/P = 0.2$ . This indicates that the wavelength dependence of the nonlinearity counteracts the temporal broadening induced by the dispersion. As was discussed in Section , the form of the nonlinearity as a function of the wavelength is similar for all the fiber geometries, only the steepness of  $\gamma(\lambda)$  decreases for decreasing  $d/P$ , whereas the form of the dispersion as a function of the wavelength is completely different for all fiber geometries. From Fig. 3(a) one can see that the temporal broadening of the pulses is reduced for all fiber geometries, only for  $d/P = 0.2$  the effect has vanished, due to the slight steepness of the nonlinearity curve.

The magnitude of the chirping is not strongly affected when the wavelength dependence of the parameters is included, but it shows a clear asymmetry that can be seen in Figs. 2(c) and 3(d). The chirp magnitudes for the geometries with  $P = 2 \mu\text{m}$ ,  $d/P = 0.2, 0.3, 0.4, 0.5, 0.6$  and for  $P = 3 \mu\text{m}$ ,  $d/P = 0.6$ , are not shown in Fig. 3(d) since the chirps are linear across the total length of the pulse and thus exhibit no relevant minima.

It can be seen from Fig. 3 that the pulses broaden more when  $d/P$  increases or  $P$  decreases, because the nonlinear and dispersion parameters increase with increasing  $d/P$  and/or decreasing  $P$ . For fiber geometries that have large periods, the  $d/P$  has less effect on the pulse broadening, because the dispersion and nonlinearity of large  $d/P$  geometries do not depend strongly on  $P$ . The geometries with small  $P$  and  $d/P$  are not suitable for short pulse amplification since the broadening of the pulses is so strong. Also, the chirping lowers the quality of the pulses and effects dispersion compensation schemes.

The amplification in the 10 cm of the fiber amplifier was calculated as

$$G = \frac{\int_{-\infty}^{\infty} |A(z, t)|^2 dT}{\int_{-\infty}^{\infty} |A(z = 0, t)|^2 dT} \quad (9)$$

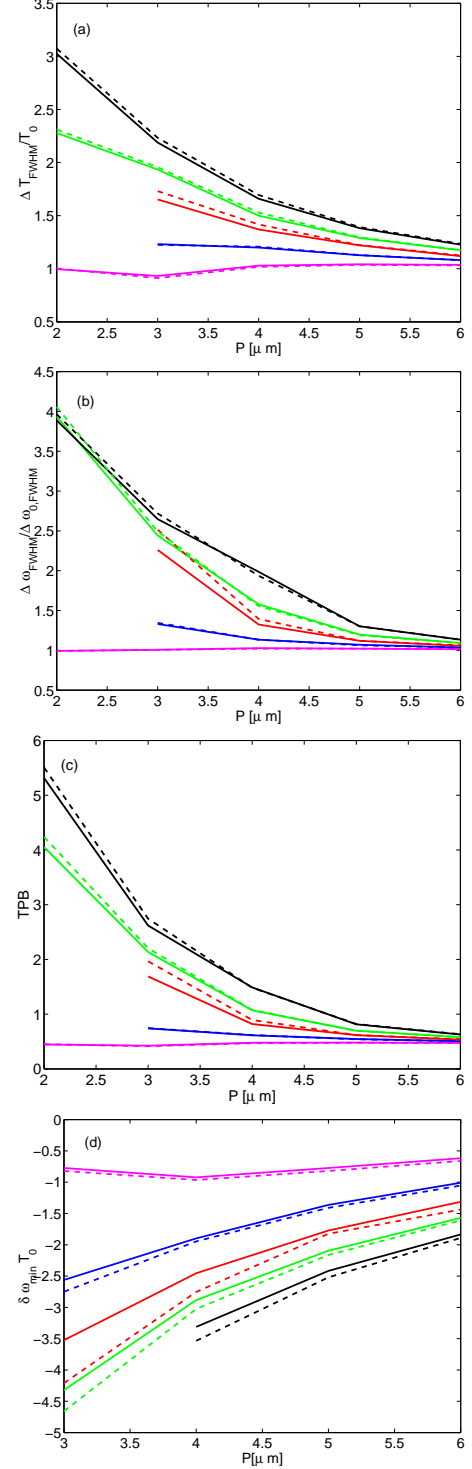


FIG. 3: (a) Temporal full-width at half-maximum, (b) spectral full-width at half-maximum, (c) time-bandwidth product, and (d) chirp of the pulses after propagating 10 cm in the fiber amplifier for the different fiber geometries:  $d/P = 0.2$  (magenta curves),  $d/P = 0.3$  (blue curves),  $d/P = 0.4$  (red curves),  $d/P = 0.5$  (green curves), and  $d/P = 0.6$  (black curves) as a function of the period  $P$ . Solid curves represent the simulations for which the wavelength dependence of  $g$ ,  $\gamma$ , and  $\beta_m$  is taken into account. Dashed curves represent the simulations where these parameters are constant. The pulse widths are scaled by the width of the initial Gaussian pulse. The chirp is the lowest value of the chirp [compare to Fig. 2(d)].

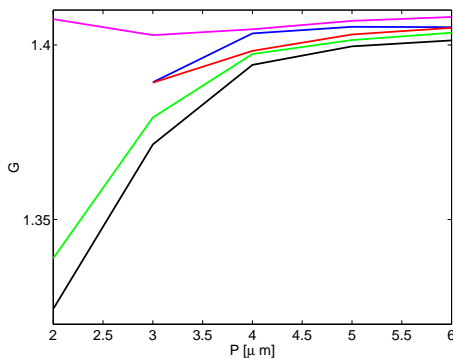


FIG. 4: The amplification of the pulses after propagating 10 cm in the fiber amplifier for the different fiber geometries:  $d/P = 0.2$  (magenta curve),  $d/P = 0.3$  (blue curve),  $d/P = 0.4$  (red curve),  $d/P = 0.5$  (green curve), and  $d/P = 0.6$  (black curve) as a function of the period  $P$ .

and it is shown in Fig. 4. Here the wavelength dependence of the parameters is taken into account. The fibers with small  $P$  and/or large  $d/P$  are amplified less since the spectrum of the pulses broadens heavily and not all frequency components get amplified since the Erbium gain spectrum is so limited. This indicates that the effects of pulse spectrum broadening have to be taken into account when high-gain fiber amplifiers are designed.

The results of two fiber geometries ( $d/P = 0.3$ ,  $P = 2 \mu\text{m}$  and  $d/P = 0.4$ ,  $P = 2 \mu\text{m}$ ) are not shown in Figs. 3 and 4. These fiber geometries have very large third order dispersion which results in a complicated pulse shape (see Fig. 5). The behavior of these pulses is completely different for the two simulations with constant and wavelength dependent parameters (compare the blue and red dashed curves in Fig. 5). Generally, when  $P$  is small, the parameters  $\beta$  and  $\gamma$  depend strongly on the wavelength, and they cannot be approximated by constant values.

#### COMPARISON OF THE IMPACT OF THE WAVELENGTH DEPENDENCE OF THE DIFFERENT FIBER PARAMETERS

In order to compare the effect of including the wavelength dependence of the different fiber parameters on the pulse characteristics, we calculated the pulse propagation for the fiber geometries  $d/P = 0.4$  and  $d/P = 0.5$  with two new sets of simulations. Firstly, we approximated the dispersion parameters  $\beta_m$  with constant values, and secondly, we approximated all other parameters, except gain, with constant values. The time-bandwidth products are shown in Fig. 6. From Fig. 6(a) one can see that the results for the simulations where all the parameters were wavelength dependent (blue squares) and where dispersion parameters  $\beta_m$  were approximated by constant values (red stars) are very close, compared to the simulations with all parameters constant (black cir-

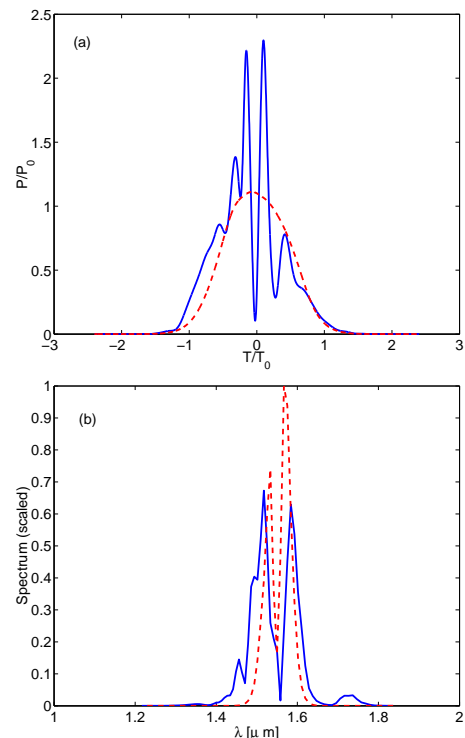


FIG. 5: (a) Pulse shape and (b) spectrum after propagating 9 cm in the fiber amplifier with geometry  $d/P = 0.4$  and  $P = 2 \mu\text{m}$ . Blue and red dashed curves represent the simulation with wavelength dependent and constant parameters  $g$ ,  $\gamma$ ,  $\beta_m$ , respectively.

cles). This indicates that the wavelength dependence of the dispersion coefficients  $\beta_m$  does not have as significant effect to the pulse as the wavelength dependence of the nonlinearity coefficient. For the fiber geometries in Fig. 6(b) the wavelength dependence of the dispersion has a larger impact on the pulse characteristics, since the pulse spectrum for the geometries with larger  $d/P$  is wider.

To determine the effect of the wavelength dependence of gain, we calculated the pulse propagation when only the wavelength dependence of gain was taken into account but all other parameters ( $\beta_m$  and  $\gamma$ ) were constant. The time-bandwidth products are shown in Fig. 6. One can see in Fig. 6(a) that the simulation where the wavelength dependence of gain is taken into account (green crosses) does not change the pulse properties in a significant amount compared to the simulation where all the parameters were constant (black circles). Again in Fig. 6(b) the effect of the wavelength dependence of gain is more important due to the extensive pulse broadening. This implies that the wavelength dependence of gain does not have a significant effect to the pulse propagation except in the case where the spectral broadening of the pulse is excessive. For the fiber geometry with  $d/P = 0.5$  and  $P = 2 \mu\text{m}$ , it is very important to include the wave-

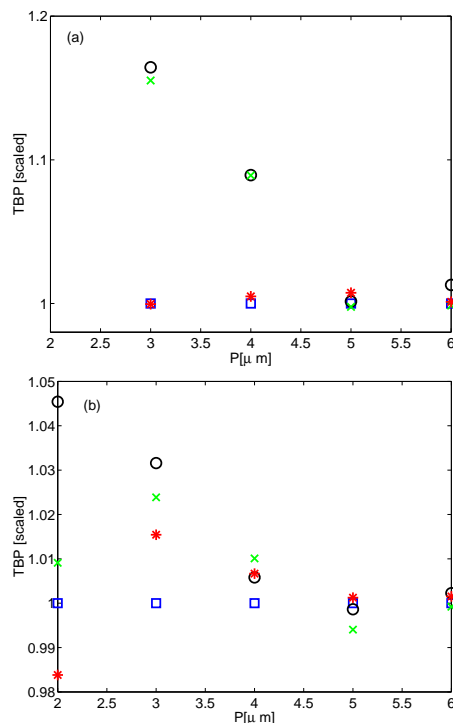


FIG. 6: Time-bandwidth products for geometries  $d/P = 0.4$  (a) and  $d/P = 0.5$  (b) as a function of the period for four different sets of simulations. Blue squares denote simulations with all parameters wavelength dependent and red stars denote simulations where dispersion constants were approximated with constant values. Black circles denote simulations with all parameters constant and green crosses denote simulations where only gain is wavelength dependent. The TBP values are scaled to the results from the simulations with all parameters wavelength dependent for the corresponding fiber geometry.

length dependence of gain in the simulation since the pulse broadens out of the gain spectrum of Erbium.

## CONCLUSIONS

We have studied pulse propagation in high-gain efficiency photonic crystal fiber amplifiers with varying periods and hole sizes. We took into account the wavelength dependence of the fiber parameters for dispersion, nonlinearity, and gain. The wavelength dependence of the fiber parameters has a significant effect on the temporal and spectral width of the pulse. The pulses were shown to broaden less for most fiber geometries when the wavelength dependence of the parameters was taken into account, indicating that the wavelength dependence of the nonlinearity counteracts the dispersion of the fibers. The spectral width and chirp showed asymmetry after propagating a short distance in the fiber amplifier. This could affect for example pulse compression or dispersion compensation schemes. Although the changes in the pulse

properties shown here were qualitatively small, they are important since the propagation distance was short compared to actual amplifier lengths. The wavelength dependence of dispersion and gain was shown not to have as profound effect on the pulse quality as the wavelength dependence of nonlinearity. However, the wavelength dependence of all fiber parameters have to be included in the simulations when the pulse spectrum broadens heavily.

## Acknowledgments

We thank Emil Aaltonen foundation and the Academy of Finland for support (Project Nos. 53903, 205454).

\* Electronic address: anu.huttunen@hut.fi

- [1] J. C. Knight, T. A. Birks, P. St. J. Russell, and D. M. Atkin, “All-silica single-mode optical fiber with photonic crystal cladding”, *Opt. Lett.* **21**, 1547–1549 (1996).
- [2] J. C. Knight, J. Broeng, T. A. Birks, and P. St. J. Russell, “Photonic band gap guidance in optical fibers”, *Science* **282**, 1476–1478 (1998).
- [3] W. J. Wadsworth, J. C. Knight, W. H. Reeves, P. St. J. Russell, and J. Arriaga “Yb<sup>3+</sup>-doped photonic crystal fibre laser” *Electron. Lett.* **36**, 1452–1454 (2000).
- [4] K. Furusawa, T. M. Monro, P. Petropoulos, and D. J. Richardson, “Modelocked laser based on ytterbium doped holey fibre,” *Electron. Lett.* **37**, 560–561 (2001).
- [5] J. K. Sahu, C. C. Renaud, K. Furusawa, R. Selvas, J. A. Alvarez-Chavez, D. J. Richardson, and J. Nilsson, “Jacketed air-clad cladding pumped ytterbium-doped fibre laser with wide tuning range,” *Electron. Lett.* **37**, 1116–1117 (2001).
- [6] K. Furusawa, A. Malinowski, J. H. V. Price, T. M. Monro, J. K. Sahu, J. Nilsson, and D. J. Richardson, “Cladding pumped Ytterbium-doped fiber laser with holey inner and outer cladding,” *Opt. Express* **9**, 714–720 (2001).
- [7] P. Glas and D. Fischer, “Cladding pumped large-mode-area Nd-doped holey fiber laser,” *Opt. Express* **10**, 286–290 (2002).
- [8] W. J. Wadsworth, R. M. Percival, G. Bouwmans, J. C. Knight, and P. St. J. Russell, “High power air-clad photonic crystal fibre laser,” *Opt. Express* **11**, 48–53 (2003).
- [9] J. Limpert, T. Schreiber, S. Nolte, H. Zellmer, T. Tünnemann, R. Iliew, F. Lederer, J. Broeng, G. Vienne, A. Petersson, and C. Jakobsen, “High-power air-clad large-mode-area photonic crystal fiber laser,” *Opt. Express* **11**, 818–823 (2003).
- [10] J. Canning, N. Groothoff, E. Buckley, T. Ryan, K. Lyytikäinen, and J. Digweed, “All-fibre photonic crystal distributed Bragg reflector (PC-DBR) fibre laser,” *Opt. Express* **11**, 1995–2000 (2003).
- [11] A. Argyros, M. A. van Eijkelenborg, S. D. Jackson, and R. P. Mildren, “Microstructured polymer fiber laser,” *Opt. Lett.* **29**, 1882–1884 (2004).

- [12] F. C. McNeillie, E. Riis, J. Broeng, J. R. Folkenberg, A. Petersson, H. Simonsen, and C. Jakobsen, "Highly polarized photonic crystal fiber laser," *Opt. Express* **12**, 3981–3987 (2004).
- [13] M. Moenster, P. Glas, G. Steinmeyer, and R. Iliev, "Mode-locked Nd-doped microstructured fiber laser," *Opt. Express* **12**, 4523–4528 (2004).
- [14] A. Mafi, J. V. Moloney, D. Kouznetsov, A. Schülzgen, S. Jiang, T. Luo, and N. Peyghambarian, "A Large-core compact high-power single-mode photonic crystal fiber laser," *IEEE Photon. Tech. Lett.* **16**, 2595–2597 (2004).
- [15] K. Furusawa, T. Kogure, J. K. Sahu, J. H. Lee, T. M. Monro, and D. J. Richardson, "Efficient low-threshold lasers based on an erbium-doped holey fiber," *IEEE Photon. Tech. Lett.* **17**, 25–27 (2005).
- [16] J. Limpert, N. Deguil-Robin, I. Manek-Hönninger, F. Salin, F. Röser, A. Liem, T. Schreiber, S. Nolte, H. Zellmer, A. Tünnermann, J. Broeng, A. Petersson, and C. Jakobsen, "High-power rod-type photonic crystal fiber laser," *Opt. Express* **13**, 1055–1058 (2005).
- [17] J. H. V. Price, K. Furusawa, T. M. Monro, L. Lefort, and D. J. Richardson, "Tunable, femtosecond pulse source operating in the range 1.06–1.33  $\mu\text{m}$  based on an  $\text{Yb}^{3+}$  doped holey fiber amplifier," *J. Opt. Soc. Am. B* **19**, 1286–1294 (2002).
- [18] A. Cucinotta, F. Poli, S. Selleri, L. Vincetti, and M. Zoboli, "Amplification properties of  $\text{Er}^{3+}$ -doped photonic crystal fibers," *J. Lightwave Tech.* **21**, 782–788 (2003).
- [19] K. G. Hougaard, J. Broeng, and A. Bjarklev, "Low pump power photonic crystal fibre amplifiers," *Electron. Lett.* **39**, 599–600 (2003).
- [20] J. Limpert, A. Liem, M. Reich, T. Schreiber, S. Nolte, H. Zellmer, A. Tünnermann, J. Broeng, A. Pettersson, and C. Jakobsen, "Low-nonlinearity single-transverse-mode ytterbium-doped photonic crystal fiber amplifier," *Opt. Express* **12**, 1313–1319 (2004).
- [21] K. Furusawa, T. Kogure, T. M. Monro, and D. J. Richardson, "High gain efficiency amplifier based on an erbium doped aluminosilicate holey fiber," *Opt. Express* **12**, 3452–3458 (2004).
- [22] A. Cucinotta, F. Poli, and S. Selleri, "Design of Erbium-doped triangular photonic-crystal-fiber-based amplifiers," *IEEE Photon. Tech. Lett.* **16**, 2027–2029 (2004).
- [23] C. Li, Y. Huang, W. Zhang, Y. Ni, and J. Peng, "Amplification properties of erbium-doped solid-core photonic bandgap fibers," *IEEE Photon. Tech. Lett.* **17**, 324–326 (2005).
- [24] A. Shirakawa, J. Ota, M. Musha, K. Nakagawa, K. Ueda, J. R. Folkenberg, and J. Broeng, "Large-mode-area erbium-ytterbium-doped photonic-crystal fiber amplifier for high-energy femtosecond pulses at 1.55  $\mu\text{m}$ ," *Opt. Express* **13**, 1221–1227 (2005).
- [25] R. Hainberger and S. Watanabe, "Impact of the wavelength dependence of the mode field on the nonlinearity coefficient of PCFs," *IEEE Photon. Tech. Lett.* **17**, 70–72 (2005).
- [26] G. P. Agrawal, *Nonlinear Fiber Optics*, (Academic, London, 1995).
- [27] A. Huttunen and P. Törmä, "Optimization of dual-core and microstructure fiber geometries for dispersion compensation and large mode area," *Opt. Express* **13**, 627–635 (2005).
- [28] S. G. Johnson and J. D. Joannopoulos, "Block-iterative frequency-domain methods for Maxwell's equations in a planewave basis," *Opt. Express* **8**, 173–190 (2001).